Title
Toward a low-cost high-voltage sodium aqueous rechargeable battery

Authors
Lee, Myeong Hwan
Kim, Sung Joo
Chang, Donghee
et al.

Publication Date
2019-10-01

DOI
10.1016/j.mattod.2019.02.004

Peer reviewed

ELSEVIER

Toward a low-cost high-voltage sodium aqueous rechargeable battery

Myeong Hwan Lee [1,†], Sung Joo Kim [1,†], Donghee Chang [1], Jinsoo Kim [2], Sehwan Moon [1], Kyungbae Oh [1], Kyu-Young Park [1], Won Mo Seong [1], Hyeokjun Park [1], Giyun Kwon [1], Byungju Lee [1], Kisuk Kang [1,3,*]

[1] Department of Materials Science and Engineering, Research Institute of Advanced Materials, Seoul National University, 1 Gwanak-ro, Gwanak-gu, Seoul 08826, Republic of Korea
[2] Environment & Energy Reseach Team, Automotive Research & Development Division, Hyundai Motor Company, Uiwang 437-815, Republic of Korea
[3] Center for Nanoparticle Research at Institute for Basic Science (IBS), Seoul National University, 1 Gwanak-ro, Gwanak-gu, Seoul 08826, Republic of Korea

Recent discovery of high-concentration electrolyte systems has opened a new avenue toward the high-voltage, safe, and low-cost aqueous rechargeable batteries. However, the need for generally high-cost organic solutes in the high-concentration electrolyte has become another major obstacle. Herein, we revisited all the commonly used low-cost solutes for high-concentration system and discovered that the use of $NaClO_4$ solute effectively results in a wide electrochemical stability window by suppressing water decomposition and induces stable solid-electrolyte interphase (SEI) layer formation without involving the reduction of salt anions. The SEI layer, composed of Na_2CO_3 and Na—O compounds including NaOH, guarantees the excellent electrochemical storage stability of the full-cell composed of $Na_4Fe_3(PO_4)_2(P_2O_7)$ cathode and $NaTi_2(PO_4)_3$ anode for the extended period of time. This new class of electrolyte systems provides remarkable cycle stability and a coulombic efficiency of ~99% at 1C for over 200 cycles, which outperforms the state-of-the-art super-concentrated systems based on $NaCF_3SO_3$.

Introduction

With the ever-increasing demand for greener and sustainable energy utilization, rechargeable batteries have received extensive attention for use in grid-scale energy storage systems (ESSs) owing to their high energy density, compactness, versatility, low maintenance, and high round-trip efficiency [1–4]. Despite the promising outlook for conventional lithium-ion batteries, many obstacles to their use for such large-scale applications have yet to be overcome, including rising costs stemming from the limited abundance of raw materials and safety concerns arising from the use of highly flammable organic electrolytes [5–10]. As an alternative safer chemistry, the batteries that employ aqueous electrolytes have been investigated owing to their non-flammability along with non-toxicity and low cost. However, traditional aqueous electrolytes provide a narrow electrochemical stability window of ~1.23 V; thermodynamic water decomposition, such as hydrogen and oxygen evolution, occurs outside this window. This narrow stability window inevitably serves as a bottleneck for the selection of electrode materials, yielding limited energy density for aqueous systems, which make them unfit for practical application [11–13]. Recently, highly concentrated electrolytes have emerged as a potential game changer in the battery market for both aqueous and non-aqueous systems because of their remarkable characteristics, which are distinct from those of conventional electrolyte systems, including low flammability, low solvent activity, and high chemical stability, that suppress side reactions [14–20]. In

* Corresponding author at: Department of Materials Science and Engineering, Research Institute of Advanced Materials, Seoul National University, 1 Gwanak-ro, Gwanak-gu, Seoul 08826, Republic of Korea.
E-mail address: Kang, K. (matlgen1@snu.ac.kr).
† These authors contributed equally to this paper.

https://doi.org/10.1016/j.mattod.2019.02.004

particular, super-concentrated electrolytes in an aqueous electrolyte system, with "water-in-salt" and "hydrate-melt" prototypes, have already outperformed conventional electrolytes by suppressing water activity, changing solvation structure with ion aggregation, and thereby expanding the electrochemical stability window with suppressed oxygen and hydrogen evolution reactions [21–33]. These newly proposed concentrated electrolytes enable high-voltage operation of aqueous batteries for a wider selection of electrodes. Nevertheless, significant economic concerns have delayed the commercialization of aqueous systems, especially regarding the use of costly solutes, which have been known to be effective in stabilizing the high-concentration electrolyte. For instance, the price of an aqueous electrolyte solution of 21 molal (21 m) lithium bis(trifluoromethanesulfonyl)imide (LiTFSI), which is the most widely studied lithium-based electrolyte system, is approximately 18 times that of conventional non-aqueous electrolytes (e.g., 1 M $LiPF_6$) [24] and about 6 times higher than that of 9.26 m $NaCF_3SO_3$, which is a well-studied sodium-based electrolyte system (see Table S1 for the cost comparison of various high-concentration electrolyte systems), signifying the urgent need for the discovery and development of low-cost, high-voltage aqueous electrolytes.

Historically, lithium- and sodium-based salts, consisting of sulfate (SO_4), nitrate (NO_3), and perchlorate (ClO_4) groups, have been primarily used as solutes for aqueous electrolytes due to their anion stability within the operating voltage window and low cost [11–13,34–37]. However, these inorganic salts have been less highlighted for their use in highly concentrated aqueous batteries than their organic counterparts, partly because it is believed that the anion decomposition of the solutes plays an important role in forming a protective SEI layer on the electrode and offering the stability of the system [26–33,38,39]. Even so, their low cost and electrochemical stability make them still worthy to be investigated. Moreover, the ability to change the water solvation structure and their solvating behaviors in the aqueous systems has been relatively well studied and documented in the previous literatures [34–37]. For example, the solvation interactions between water molecules and inorganic salt ions dissolved in water are well represented by the Hofmeister series, which ranks the role of salt ions in the aqueous solvation process according to their water solvation strength [40]. While the series is originally used to examine the influence of the salts on the solubility of proteins in water and has been studied in the dilute conditions, it may as well be extended to predict the effects of inorganic salts on the solvation structure in the aqueous solution. Further, rank-ordering various anions and dividing them into water-structure-making and breaking groups from the series might offer the guidelines in the selection of the proper solutes in high-concentration aqueous electrolytes. Anion salts that have a strong tendency to break the water structure would be correlated with the solubility and the probability of changing solvation structures with ion aggregations [36,37,41]. Recent molecular dynamics (MD) simulations also support that this would be more pronounced in the case of highly concentrated aqueous solutions [42–47]. These theoretical studies suggested that high-concentration water-structure-breaking salts tend to exhibit ion-aggregated networking with water, enhancing the possibility of expanding the stability voltage window of aqueous electrolytes.

In the present work, we carefully examine these commonly used low-cost solutes in the high-concentration systems and revisited their chemistry in the rechargeable aqueous batteries. Water-structure-modifying effect of the salts was probed for saturated aqueous solutions in which lithium- or sodium-sulfate (SO_4), nitrate (NO_3), and perchlorate (ClO_4) solutes were dissolved and was compared with those of already reported super-concentrated electrolytes using organic salts, such as LiTFSI and $NaCF_3SO_3$. We also unveiled that saturated $NaClO_4$ (17 m) solution is a promising candidate for a low-cost, high-voltage sodium aqueous electrolyte with an electrochemical stability window of ~2.7 V. Using this new class of electrolyte, we successfully developed a Na-ion full-cell with high coulombic efficiency (~99%) and cycle stability for up to 200 cycles at 1C. In addition, it is demonstrated that a highly concentrated electrolyte composed of $NaClO_4$ forms a remarkably stable SEI layer without anion decomposition, with extraordinary open-circuit voltage (OCV) stability for ~900 h.

Experimental section

Material synthesis

Aqueous electrolytes, including $NaClO_4$ solution, of varying molality (the number of moles of salt (solute) per kilograms of solvent, here denoted by m) were prepared with concentrations marked in abbreviation (1 m, 5 m, 10 m, and 17 m $NaClO_4$). Other saturated aqueous solutions were also prepared by molality, which include 1.3 m Na_2SO_4, 10.7 m $NaNO_3$, 21 m LiTFSI, and 9.26 m $NaCF_3SO_3$. $Na_4Fe_3(PO_4)_2(P_2O_7)$ was synthesized via a conventional solid-state method. Stoichiometric quantities of $Na_4P_2O_7$ (95%, Aldrich), $FeC_2O_4{\cdot}2H_2O$ (99%, Aldrich), and $NH_4H_2PO_4$ (98%, Aldrich) were mixed using high-energy ball milling (Pulverisette 5, FRITSCH) at 400 rpm for 12 h. The mixture was calcined at 300 °C for 6 h under flowing argon (Ar) before being manually pelletized under 200 kg cm^{-2} pressure using a disk-shaped mold. The pellets were then sintered again at 550 °C for 12 h under flowing Ar. To enhance the electrical conductivity of the electrode, pyromellitic acid (PA) ($C_{10}H_6O_2$, 96%, Alfa Aesar) was added during ball milling (weight ratio of active material:PA = 95:5).

Similarly, a $NaTi_2(PO_4)_3$ anode was synthesized by mixing stoichiometric amounts of Na_2CO_3 (98%, Aldrich), TiO_2 (99.7%, anatase phase, Aldrich), and $(NH_4)_2HPO_4$ (98%, Aldrich) via ball milling in acetone for 24 h before evaporation at 70 °C for 12 h. The homogeneously mixed powder was sintered at 300 °C for 6 h under flowing Ar. The calcined powder was manually pelletized under 200 kg cm^{-2} pressure using a disk-shaped mold. The pellets were then heated again at 900 °C for 24 h in air. The carbon-coated $NaTi_2(PO_4)_3$ was prepared via high-energy ball milling at 400 rpm for 2 h with PA (weight ratio of active material:PA = 95:5). The mixture was annealed at 800 °C for 2 h under Ar flow.

Electrochemical measurements

A $Na_4Fe_3(PO_4)_2(P_2O_7)$ electrode was fabricated by compressing the mixture of active materials, Super P carbon black, and polytetrafluoroethylene (PTFE) binder with a mass ratio of 7:2:1

against a stainless-steel grid. A $NaTi_2(PO_4)_3$ electrode was similarly fabricated with a mass ratio of 8:1:1 on a stainless-steel grid. Cyclic voltammetry (CV) was performed using a three-electrode system at a scan rate of 1 mV s^{-1} with a gold electrode (area of 0.126 cm^2) as the working electrode, a standard calomel electrode (SCE) as the reference electrode, and Pt wire as the counter electrode. For galvanostatic measurements, a half-cell was assembled using a three-electrode configuration with the active electrode as the working electrode, activated carbon as the counter electrode, and a SCE as the reference electrode. The full-cell was assembled in a coin-type electrochemical cell (CR2032, Wellcos). Galvanostatic measurements of the half-cell and full-cell were conducted using a multichannel potentio-galvanostat (WBCS-3000, Wonatech, Korea) at 25 °C. The entire preparation process was carried out in a nitrogen-filled glove box.

Material characterization

Raman spectroscopy (LabRAM HR Evolution, Horiba) was conducted using capillary tubes (inner diameter of 1.1–1.2 mm) with a continuous wave linearly polarized laser wavelength of 532 nm. Surface analysis of $NaTi_2(PO_4)_3$ was conducted using transmission electron microscopy (TEM; JEM-2100F, JEOL) and electron energy loss spectroscopy (EELS; Quantum 963, Gatan, Inc, USA). X-ray photoelectron spectroscopy (XPS) analysis was performed using a monochromatic Al K_α X-ray source (1486.6 eV) generated by an acceleration voltage of 15 kV (PHI 5000 VersaProbe, ULVAC-PHI). XPS spectra of all the electrodes were obtained with a raster size of 2×2 mm^2 after the etching of the electrodes using Ar^+-sputtering at a 2-kV acceleration voltage. All the electrodes were etched less than 5 nm by Ar ion-sputtering to reduce the damage from Ar^+ etching and to properly determine the composition of the SEI layer on the electrode surface. The overall XPS peaks were arranged based on the reference C—C bond at 284.4 eV.

Soft X-ray absorption spectroscopy (sXAS) measurements were performed at the 10D KIST bending magnet beamline of the Pohang Light Source-II (PLS-II) at room temperature under a base pressure of 3×10^{-10} torr. Spectra of the C and O K-edges were obtained in surface-sensitive total electron yield (TEY) mode at a penetration depth of <10 nm and normalized to the incident photon flux at an energy resolution of 0.1 eV. Before the measurements, all the electrode samples were washed with 1, 2-dimethoxyethane (DME) many times and then dried in a vacuum chamber at 70 °C for 12 h. The structures and morphologies of both pristine $Na_4Fe_3(PO_4)_2(P_2O_7)$ and $NaTi_2(PO_4)_3$ powders were examined using X-ray diffraction (XRD; New D8 Advance, Bruker) and scanning electron microscope (SEM; SUPRA 55VP, Carl Zeiss).

Results

In search of new super-concentrated aqueous electrolytes, the following criteria were carefully considered: (1) high intrinsic solubility that results in a cation/water ratio > 0.3 to eliminate free water, (2) wide availability with potentially low cost, and (3) the ability to change a cation–anion–water molecule solvation structure to an ion-aggregated structure, which can lead to low water activity based on previous reports [22,26–28,31,38,39]. In addition, we referred to the Hofmeister series in the selection, considering the water solvation strength of inorganic salts. As a result, we came up with a list of commonly used salts, including sulfate (SO_4)-, nitrate (NO_3)-, and perchlorate (ClO_4) -based sodium salts, as tabulated in Table S1. According to the Hofmeister series, the relative ability to destabilize the bulk water structure for these representative inorganic salt anions is $SO_4^{2-} < NO_3^- < ClO_4^-$, implying that ClO_4^- salts have a strong tendency to break the water structure, indicating the probability of changing solvation structures with ion aggregations [36,37,41]. Moreover, it was found that the solubility of inorganic salts follows the order of water-structure-breaking strength for these salts (i.e., $SO_4^{2-} < NO_3^- < ClO_4^-$) as shown in Table S1. Upon reaching the solubility limits in water, the water-breaking ions that constitute the higher end of the rank order (i.e., ClO_4^-) are predicted to be capable of forming complex ion networks with the water structure, disrupting their hydrogen-bonding networks [36,37,40,41,46,47].

To verify this prediction, Raman spectroscopy was employed as a tool to identify the fingerprints from changes in the solvation structure of the electrolyte candidates depending on the salt concentrations. Fig. 1a and b present the spectra of O—H stretching vibration modes of water molecules for the series of lithium and sodium aqueous electrolyte candidates at varying salt concentrations in the band range of 2700–4000 cm^{-1} (see Fig. S1 for more extended data in Supporting Information). For deionized (DI) water and low-concentration electrolytes, both the symmetric (near 3200 cm^{-1}) and asymmetric (near 3400 cm^{-1}) vibration modes of water molecules exhibit a broad Raman band due to their diverse hydrogen-bonding environments [22,31,48,49]. The broad band of water clusters maintains its shape at wide ranges of salt concentrations for electrolytes containing Na_2SO_4, $NaNO_3$, Li_2SO_4, $LiNO_3$ and $LiClO_4$ (Fig. S1), indicating the major presence of free water. Even at the saturated concentrations of these salts in the electrolyte, the broad nature of the band did not notably change in contrast to the behavior of well-known super-concentrated salts of $NaCF_3SO_3$ and LiTFSI in Fig. 1a. On the other hand, it was found that $NaClO_4$ exhibit hydration characteristics that are distinct from those of other conventional electrolytes and are similar to those of $NaCF_3SO_3$ and LiTFSI. Fig. 1b illustrates that, with increasing salt concentration of $NaClO_4$, the O—H stretching vibration bands are significantly altered, with gradual disappearance of the broad band followed by the rise of a sharp peak near 3550 cm^{-1}, which resembles the characteristics of "water-in-salt" [22,31,50]. Moreover, $NaClO_4$ showed the most pronounced blue shift of the Raman band, even close to that of LiTFSI, which has been reported as one of the most effective salts in stabilizing the water in the electrochemical system [26–28,31,38]. According to the literatures, this new sharp peak near 3550 cm^{-1} was attributed to the signature of crystalline hydrates, where most water molecules participate in ion coordination with cations and anions of the salt with negligible hydrogen bonding among them, giving rise to a unique solvation structure.

Inspired by this observation, we examined more carefully the aggregation behavior of the $NaClO_4$ salts in the electrolyte at various concentrations based on the change in the ClO_4^- stretching bands in Raman spectra (Fig. 1c). It was found that the overall

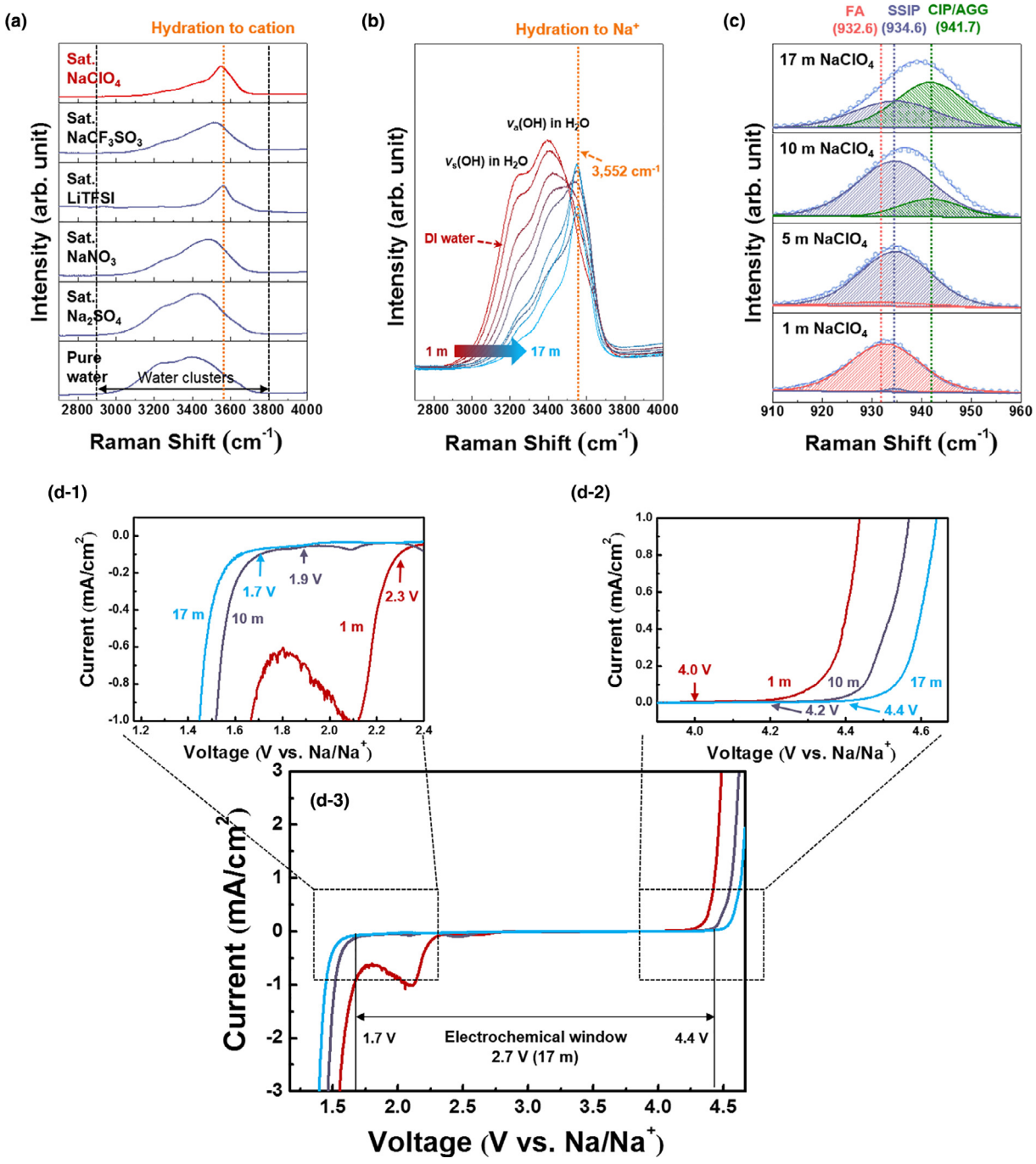

FIGURE 1

(a) Raman spectra of water molecules in various aqueous solutions, namely, saturated 1.3 m Na_2SO_4, saturated 10.7 m $NaNO_3$, saturated 21 m LiTFSI, saturated 9.26 m $NaCF_3SO_3$, and saturated 17 m $NaClO_4$ in water. The broadening of the spectra between the two black dashed lines in the range of 2900–3800 cm^{-1} is attributed to O—H stretching modes of clustered water molecules with diverse hydrogen bonding. The sharp peak marked by the orange line near 3550 cm^{-1} is attributed to cation-solvated water molecules that are free of hydrogen bonding. (b) Raman spectra of $NaClO_4$ electrolyte at various salt concentrations in the range of 2700–4000 cm^{-1} showing O—H stretching modes of water molecules. (c) ClO_4 stretching modes in Raman spectra for $NaClO_4$ electrolytes of different salt concentrations (1 m, 5 m, 10 m, and 17 m). (d-3) Overall electrochemical stability window and (d-1 and 2) enlarged regions near the cathodic (HER) and anodic (OER) limits of 17 m $NaClO_4$ electrolyte determined from CV measurements between −1.55 and 1.65 V *vs.* SCE at 1 mV s^{-1} on gold working electrodes. The potential was converted to a Na/Na^+ reference for convenience. The bump near 2.1 V *vs.* Na/Na^+ in (d) is attributed to bubble formation on a gold electrode.

band spectra undergo a blue shift with increasing salt concentration from 1 m to 17 m, indicating the notable change in the cation–anion coordination environment. The band can be deconvoluted into three components: free anions (FA: 932.6 cm^{-1} red dashed line), solvent-separated ion pairs (SSIP: 934.6 cm^{-1}, blue dashed line), and contact ion pairs (CIP)/aggregated cation–anion pairs (AGG: 941.7 cm^{-1}, green dashed line) (Fig. 1c and Table S2) [51]. The fraction of FA, approximately

77% at 1 m salt concentration, drastically drops to 20% at 5 m before reaching 0% at 10 m. In contrast, the fraction of SSIP increases from 22.8% at 1 m to 79.9% at 5 m concentration before dropping to 42.9% at 17 m concentration with the majority of ion species (above 57%) existing as CIP/AGG. Based on both the O—H stretching and ClO_4^- stretching band spectra, the solvation structure of the 17 m $NaClO_4$ aqueous electrolyte is believed to primarily consist of a highly ion-aggregated state with low free water content (Table S1). This finding is in line with the previous density functional theory (DFT) calculation, which predicted a significant increase in the number of large ion aggregates that break the hydrogen bonding of water by infiltrating its percolating structure in the form of an intertwined network [46,47].

The reduced water activity expected from this unique solvation chemistry can most likely be translated into widening of the electrochemical stability window. Hence, CV was performed for the 17 m $NaClO_4$ electrolytes at a scan rate of 1 mV s^{-1}, as shown in Fig. 1d. The overall stability window broadens to cathodic and anodic limits of ~1.7 V and ~4.4 V *vs.* Na/Na^+, respectively, offering a wide voltage window of 2.7 V. In the enlarged view of anodic region in Fig. 1(d-2), it is clearly shown that the oxygen evolution reaction (OER) is suppressed with increasing salt concentration from 1 m to 17 m, with the onset potential of the OER shifting from 4.0 to 4.4 V *vs.* Na/Na^+. This finding supports the reduced water activity in the high-concentration systems resulting from the changes in the solvation structure [22,26–28,31]. In addition, the limit of the cathodic side is also pushed from 2.3 to 1.7 V with the same concentration change, effectively suppressing the hydrogen evolution reaction (HER), as shown in Fig. 1(d-1). The reduced HER activity can likely be attributed to the formation of a passivation layer from the reduction of salt aggregates as previously reported for most of super-concentrated aqueous electrolyte systems [26–28,30–33,39]. However, considering the relative stability of ClO_4^- against reduction [52], this point requires further scrutiny and will be discussed later.

Based on the initial assessment of the electrochemical stability window, the electrochemical properties of both the cathode and the anode were further evaluated by employing $NaClO_4$ electrolytes. $Na_4Fe_3(PO_4)_2(P_2O_7)$ was selected as a cathode material due to its demonstrated cycle stability in the organic electrolytes [53–55]. $NaTi_2(PO_4)_3$ was selected as an anode material with its average potential of 2.1 V *vs.* Na/Na^+ [11,12,56–59]. The structures and morphologies of both pristine $Na_4Fe_3(PO_4)_2(P_2O_7)$ and $NaTi_2(PO_4)_3$ powders were examined using X-ray diffraction (XRD) and scanning electron microscope (SEM), as shown in Fig. S2. Fig. 2a and b present the electrochemical profiles of $Na_4Fe_3(PO_4)_2(P_2O_7)$ and $NaTi_2(PO_4)_3$ half-cells in 1 m and 17 m $NaClO_4$ electrolytes, comparatively. The first charge/discharge profiles of the $Na_4Fe_3(PO_4)_2(P_2O_7)$ cathode at 1C under both 1 m and 17 m conditions reveal discharge capacity of 90–100 mAh g^{-1} with an average redox voltage of ~3.2 V *vs.* Na/Na^+, which is similar to that achieved using organic electrolytes (Fig. 2a). However, charging the cathode to 4.2 V, higher than the theoretical oxygen evolution potential (3.527 V *vs.* Na/Na^+ at pH = 7), induces oxygen evolution at ~3.9 V *vs.* Na/Na^+ in the 1 m condition. On the other hand, the OER reaction is substantially suppressed in the 17 m condition, which is consistent with the CV results in Fig. 1(d-2). More dramatic difference could be found in the anodic performance. The voltage profile of the $NaTi_2(PO_4)_3$ anode in 1 m $NaClO_4$ electrolytes indicates the serious HER near 2.0 V *vs.* Na/Na^+ (Fig. 2b). This is attributable to the HER potential (2.297 V *vs.* Na/Na^+ at pH = 7) that is higher than the redox potential of $NaTi_2(PO_4)_3$, driving hydrogen evolution to occur in the conventional aqueous electrolyte simultaneously with sodiation of $NaTi_2(PO_4)_3$ near 2.1 V *vs.* Na/Na^+. However, it is remarkable that the highly concentrated $NaClO_4$ electrolyte could effectively suppress the hydrogen evolution and successfully deliver the discharge capacity of 113 mAh g^{-1} reversibly. Moreover, the capacity could be reversibly retained over 200 cycles in the 17 m $NaClO_4$ electrolyte as shown in Fig. S3.

To further evaluate the practicality of $NaClO_4$ electrolytes, $Na_4Fe_3(PO_4)_2(P_2O_7)/NaTi_2(PO_4)_3$ full-cells were assembled and tested at different electrolyte concentrations. The negative-to-positive electrode mass ratio (NP ratio) was set to ~1.1:1, considering the specific capacity of $Na_4Fe_3(PO_4)_2(P_2O_7)$ and $NaTi_2(PO_4)_3$. Fig. 2c and d present the galvanostatic charge/discharge profiles of the full-cell at 1C in 1 m and 17 m $NaClO_4$ electrolytes, respectively, within the voltage range between 0.01 and 2.0 V. In both electrolytes, the full-cell exhibited a discharge capacity of ~44 mAh g^{-1} based on the total electrode mass (denoted as mAh g_{tot}^{-1}) with an average redox voltage of 1.0 V, which is equivalent to an energy density of 36 Wh kg^{-1}. However, similar to the observations in the half-cells, the full-cell using the 1 m electrolyte exhibited irreversible capacity decay upon the first cycle owing to water decomposition that occurs at approximately 1.8 V (Fig. 2c). The water decomposition is slightly suppressed for the 1 m electrolyte as compared with the half-cells, which is attributed to a relatively fast rate (above 1C), kinetically hindering the decomposition reaction [28]. On the other hand, significantly less degradation was observed when the 17 m $NaClO_4$ electrolyte was used as shown in Fig. 2d. In consistent with the half-cell results, no signature of the OER or HER was observed, leading to reversible charge and discharge reaction. CVs of the full-cells that were carried out at a slow scan rate (0.1 mV s^{-1}) further confirm the difference in each electrolyte. The insets of Fig. 2c and d illustrate that the irreversible reaction clearly occurred above 1.8 V in the 1 m electrolyte, whereas no detectable signature of the side reaction was observed at a similar voltage level for the 17 m electrolyte.

The long-term cycle stability and coulombic efficiency of the $Na_4Fe_3(PO_4)_2(P_2O_7)/NaTi_2(PO_4)_3$ full-cell are examined in Figs. 2e and S5. The discharge capacity fading of the cell in 1 m $NaClO_4$ electrolyte was notably severe over repeated cycles, as the capacity decreases rapidly from 44 to 8 mAh g_{tot}^{-1} (or equivalently from 87 to 17 mAh g^{-1} based on the cathode mass) within only 50 times of charge and discharge. The coulombic efficiency in 1 m electrolyte was also low (Fig. S5), starting at 87% for the first cycle before plummeting to 68%. However, notable improvements in both the capacity retention and columbic efficiency of the cell were observed in 17 m electrolyte, with their values eventually reaching 75% and 99% after 200 cycles, respectively. Unexpectedly, this performance is comparable to that of the previously reported "water-in-salt" $NaCF_3SO_3$ electrolyte (capacity retention and coulombic efficiency of 63% and 99%, respectively) as shown

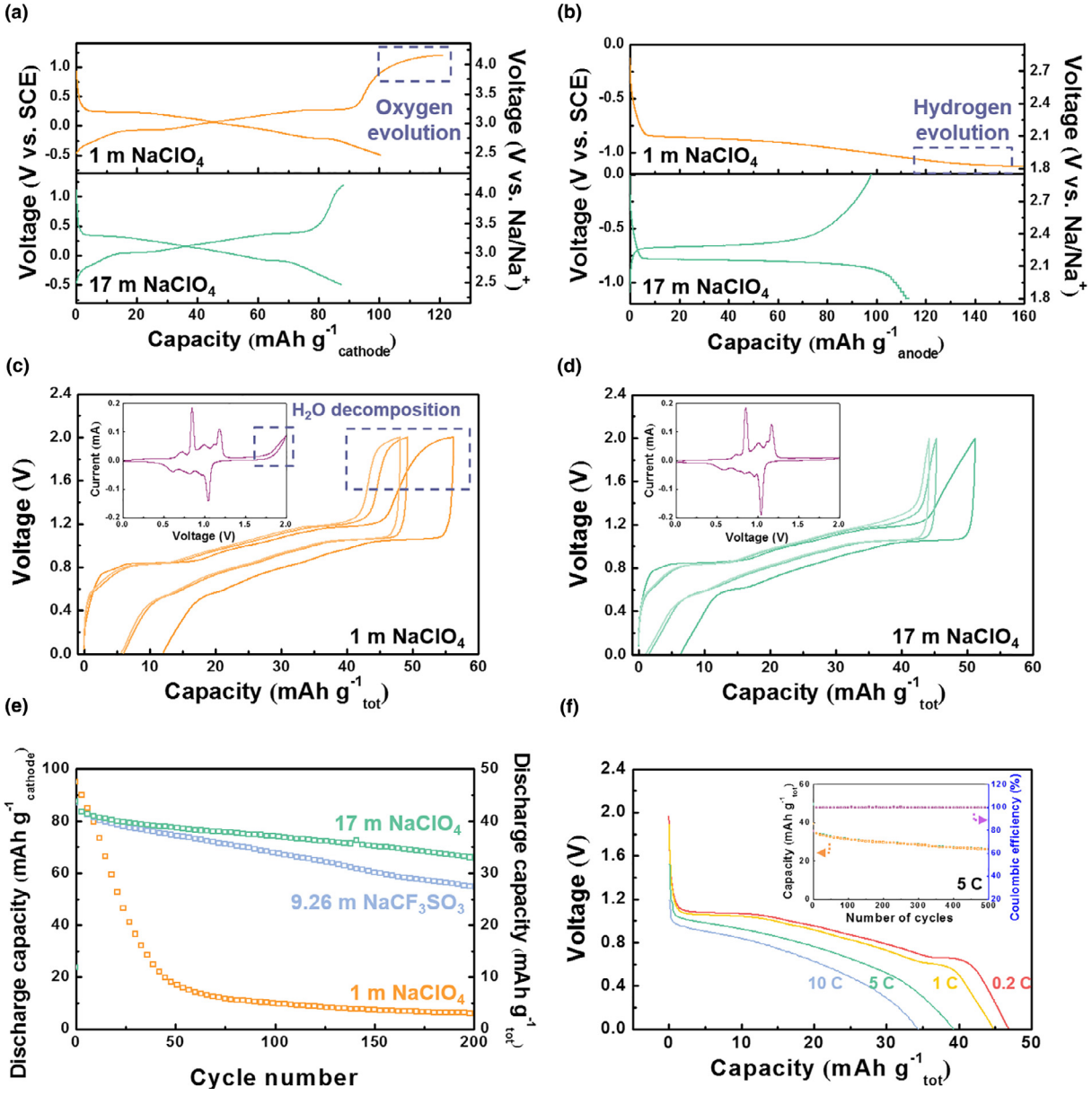

FIGURE 2

Comparison of voltage profiles of (a) $Na_4Fe_3(PO_4)_2(P_2O_7)$ electrode and (b) $NaTi_2(PO_4)_3$ electrode in 1 m and 17 m $NaClO_4$ electrolytes at constant current of 1C. The half-cell data in (a) and (b) were obtained from a three-electrode system consisting of $Na_4Fe_3(PO_4)_2(P_2O_7)$ and $NaTi_2(PO_4)_3$ as working electrodes, a SCE as the reference electrode, and activated carbon as the counter electrode. Galvanostatic profiles of the $Na_4Fe_3(PO_4)_2(P_2O_7)/NaTi_2(PO_4)_3$ full-cell in (c) 1 m and (d) 17 m $NaClO_4$ electrolytes at 1C. The insets of (c) and (d) present CV curves of the $Na_4Fe_3(PO_4)_2(P_2O_7)/NaTi_2(PO_4)_3$ full-cell at a scan rate of 0.1 mV s^{-1} in (c) 1 m and (d) 17 m $NaClO_4$ electrolytes. (e) Cycle stability of $Na_4Fe_3(PO_4)_2(P_2O_7)/NaTi_2(PO_4)_3$ full-cell cycled at 1C in different aqueous electrolytes: 1 m $NaClO_4$, 9.26 m $NaCF_3SO_3$, and 17 m $NaClO_4$. (f) Rate performance of the $Na_4Fe_3(PO_4)_2(P_2O_7)/NaTi_2(PO_4)_3$ full-cell in 17 m electrolyte at 0.2C, 1C, 5C, and 10C. The inset of (f) presents the cycle stability and coulombic efficiency of the full-cell in 17 m electrolyte at 5C. The voltage of the full-cell ranges between 0.01 and 2.0 V.

in Figs. 2e and S4 and S5. Additionally, we evaluated the rate capability of the full-cell in 17 m $NaClO_4$ electrolyte. Fig. 2f presents the discharge profiles of the full-cell at 0.2C, 1C, 5C and 10C after the first charge at 0.2C. The full-cell delivered capacities of 46, 44, 39, and 34 mAh g_{tot}^{-1} at 0.2C, 1C, 5C, and 10C, respectively. The acceptable rate capability of the full-cell is attributed to its high ionic conductivity of 108 mS cm^{-1} measured at 25 °C. Even at extended high-rate cycle tests, the cell could retain the high capacity and power capability at 5C for more than 500 cycles as illustrated in the inset of Fig. 2f.

As demonstrated thus far, the highly concentrated $NaClO_4$ electrolyte suppresses water decomposition and enhances the performance of the aqueous cell, presumably due to the change in the ion solvation structure and reduced water activity. However, it is also worth noting how it influences the stability of the electrode surface, as it has been widely suggested that the formation of a SEI on an active anode occurs via reduction of salts and partially negates the hydrogen evolution [26–28,30,31,39]. In addition, the passivation layer acts as a critical component in maintaining the structural stability of a $NaTi_2(PO_4)_3$ anode.

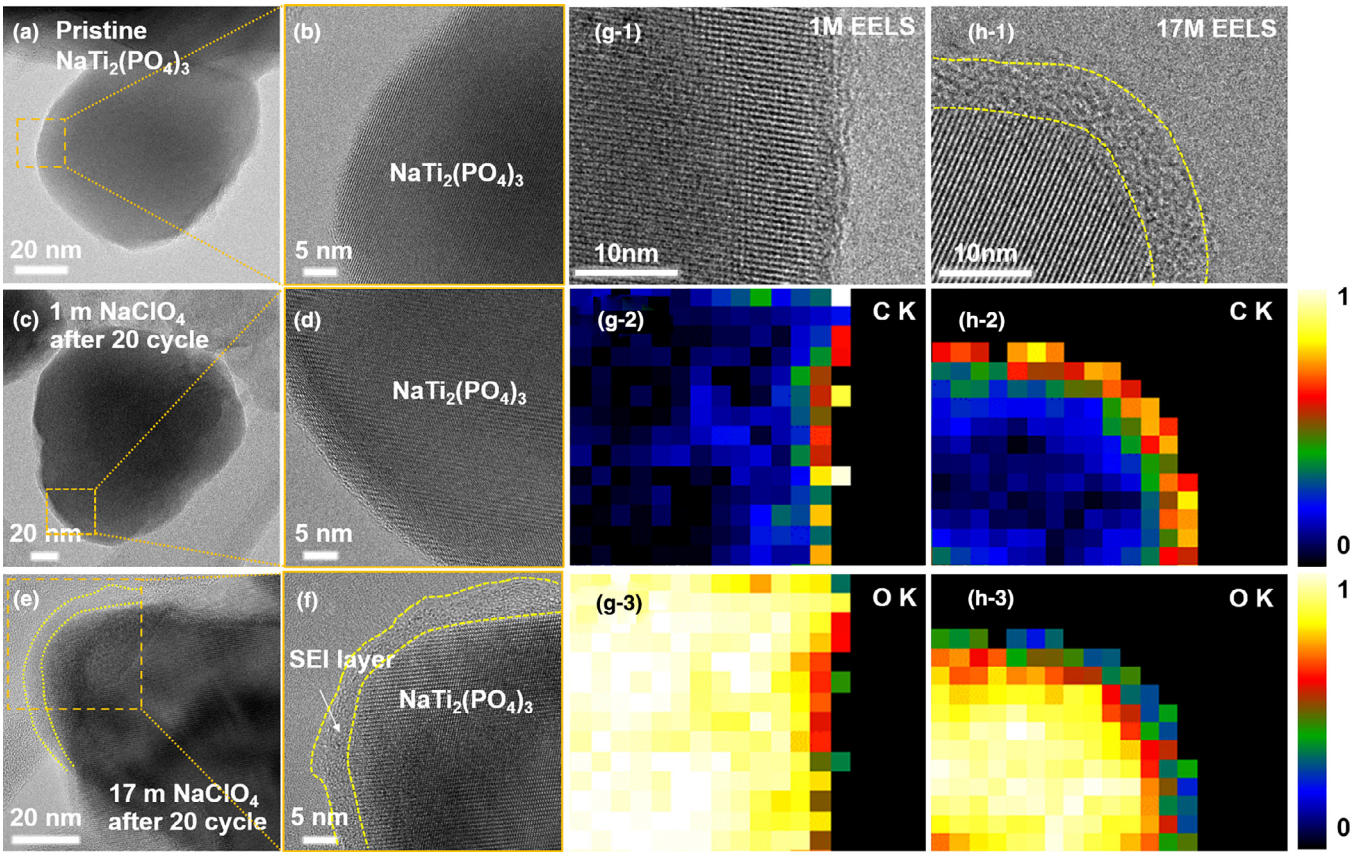

FIGURE 3

TEM analysis of a $NaTi_2(PO_4)_3$ anode surface. Low-magnification TEM images of (a) pristine $NaTi_2(PO_4)_3$ and $NaTi_2(PO_4)_3$ after 20 cycles in (c) 1 m and (e) 17 m $NaClO_4$ electrolytes at 1C. (b), (d), and (f) high-magnification TEM images of (a), (c), and (e), respectively. (g-1) High-resolution TEM images and corresponding elemental EELS maps showing (g-2) carbon K-edge and (g-3) oxygen K-edge of $NaTi_2(PO_4)_3$ surface after 20 cycles in 1 m $NaClO_4$ electrolyte. (h-1) High-resolution TEM images and corresponding elemental EELS maps of (h-2) carbon K-edge and (h-3) oxygen K-edge of $NaTi_2(PO_4)_3$ surface after 20 cycles in 17 m $NaClO_4$ electrolyte.

Nevertheless, to the best of our knowledge, ClO_4^- reduction from the $NaClO_4$ electrolyte appears highly improbable within the voltage window tested here, as it requires high decomposition energy [52]. Hence, it is necessary to verify how the $NaTi_2(PO_4)_3$ anode surface has been protected in our $NaClO_4$ electrolytes. To examine the surface of the $NaTi_2(PO_4)_3$ anode, two samples of $NaTi_2(PO_4)_3$ anodes before and after 20 cycles were prepared and probed using transmission electron microscopy (TEM). Fig. 3a–f present representative TEM images of the $NaTi_2(PO_4)_3$ electrode particles before and after 20 cycles in 1 m and 17 m $NaClO_4$ electrolytes. The pristine $NaTi_2(PO_4)_3$ particles exhibited clean surfaces with a carbon coating layer thickness of less than 1 nm (Fig. 3a and b). After cycles in 1 m $NaClO_4$ electrolyte, no significant change or formation of additional protective surface film was observed on the surface of the electrode particles (after 20 cycles at 1C), as shown in Fig. 3c and d. However, for the sample cycled in 17 m $NaClO_4$ electrolyte, a 5- to 10-nm-thick amorphous layer was observed on the $NaTi_2(PO_4)_3$ surface (Fig. 3e and f), indicating the formation of surface passivation film. The presence of the surface layer after the cycles is similar to what has been previously observed for the $NaTi_2(PO_4)_3$ anode cycled in highly concentrated $NaCF_3SO_3$ electrolyte with the SEI layer on the surface (Fig. S6). According to the previous report, it has been suggested that the SEI layer forms due to the reduction of $NaCF_3SO_3$ salts, yielding to the byproducts, such as crystalline NaF nanoparticles, which actively preserve the electrode surface from the HER reaction [28]. Nevertheless, in our extensive analysis of the surface film, we could not detect any component related with the byproducts from $NaClO_4$ decomposition within the surface layer of the electrode after cycling in the saturated electrolyte system. Moreover, no sign of elements derived from salt reduction, such as Cl, could be detected. Fig. 3g and h present the chemical composition analysis of the surface region performed for the $NaTi_2(PO_4)_3$ anode cycled in 1 m and 17 m $NaClO_4$ via EELS mapping. While a passivation layer is hardly detectable on the electrode cycled in 1 m $NaClO_4$ electrolyte in Fig. 3g, even for the thick surface film on the electrode cycled in 17 m electrolyte (light yellow dashed region in Fig. 3(h-1)), we were only able to detect carbon and oxygen K-edge signals as elements comprising the SEI layer, and other signature of salt reduction, such as Cl, could not be detected as illustrated in Figs. 3(h-2), 3(h-3), and S7.

To support TEM results, XPS analysis was performed on the $NaTi_2(PO_4)_3$ electrodes cycled in 1 m and 17 m $NaClO_4$ electrolytes to obtain an in-depth chemical view of the surface layers. O 1s, Na 1s, and Cl 2p spectra of the surfaces of the pristine and cycled electrodes are obtained in Fig. 4a–c. The figures show that

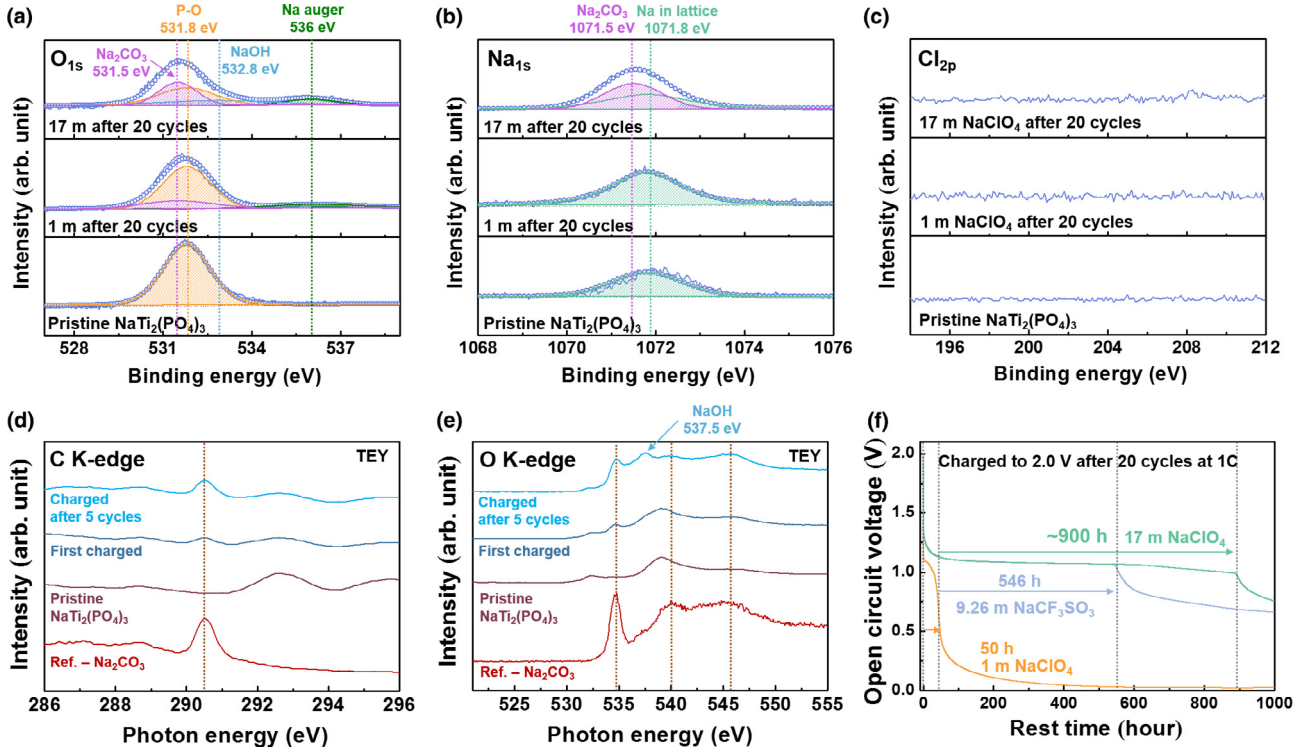

FIGURE 4

XPS profile of (a) O 1s spectra, (b) Na 1s spectra, and (c) Cl 2p spectra of the $NaTi_2(PO_4)_3$ electrode before and after 20 cycles in 1 m and 17 m $NaClO_4$ electrolyte. (d) Carbon K-edge and (e) oxygen K-edge of sXAS spectra of pristine $NaTi_2(PO_4)_3$ electrode, first charged electrode, and electrode charged after 5 cycles and reference Na_2CO_3. (f) Voltage decay curve of a $Na_4Fe_3(PO_4)_2(P_2O_7)$/$NaTi_2(PO_4)_3$ full-cell after full charge (SOC 100) measured at 25 °C. Before obtaining the voltage decay curve, the full-cell was cycled 20 times at 1C in different aqueous electrolytes: 1 m $NaClO_4$, 9.26 m $NaCF_3SO_3$, and 17 m $NaClO_4$, as shown in the graph.

O 1s and Na 1s spectra of the electrode cycled in 17 m $NaClO_4$ electrolytes present generally red shifts compared with those of the pristine electrode and the electrode cycled in 1 m $NaClO_4$ electrolyte. Peak deconvolution revealed that Na_2CO_3 (the peak at 531.5 eV in O 1s spectra and the peak at 1071.5 eV in Na 1s spectra; purple dashed line) and NaOH (the peak at 532.8 eV in the O 1s spectra, light blue dashed line) were present in the surface layer of the cycled electrode in the saturated $NaClO_4$ electrolytes (Fig. 4a and b). In addition, the Na Auger peak at 536 eV (green dashed line in Fig. 4a) in the O 1s spectra was also detected for the electrode cycled in 17 m $NaClO_4$ electrolytes. For possible production of the reduction products from $NaClO_4$, Cl 2p spectra of the electrodes are examined in Fig. 4c. It is apparent that no salt reduction occurred to generate known compounds, such as NaCl, from $NaClO_4$, which is consistent with the EELS results in Fig. S7. sXAS analysis was further employed to confirm the XPS results. In Fig. 4d and e, the surface of the $NaTi_2(PO_4)_3$ electrode at the pristine and charged states after the first and after 5 cycles in 17 m electrolyte was examined for the carbon and oxygen K-edge signals in comparison with a reference Na_2CO_3 spectrum. Both the carbon and oxygen K-edge signals that newly appeared after the first charge agree with the characteristic signals of Na_2CO_3, indicating the formation of Na_2CO_3 in 17 m $NaClO_4$ system. It is also noted that the peak corresponding to Na_2CO_3 gradually increased until the fifth cycle, implying that the surface layer forms immediately during the first charge process and continues to grow to better protect the surface from the HER. In addition, the newly appeared signal after the fifth cycle in the oxygen K-edge spectrum corresponds to the characteristic signature from NaOH, suggesting its formation on the NTP surface in 17 m $NaClO_4$ electrolyte.

Discussion

Based on the results from the surface analysis of the electrode in highly concentrated electrolytes, we propose that (1) the formation of the surface layer occurs from the first charge process and (2) the layer is composed of carbonates and hydroxides without significant contribution from the salt reduction. Previous reports on a highly concentrated lithium aqueous battery system showed that inorganic compounds, such as carbonates and oxides, other than those from salt reduction also likely form during electrochemical cycling and they usually originate from the reduction species of O_2 and CO_2 dissolved in the electrolyte [39]. Similarly, it is supposed that the surface layer formation comprising of Na_2CO_3 in the 17 m $NaClO_4$ electrolyte was possibly driven by reduction of dissolved gases (O_2 and CO_2). During the first charge process of the full-cell in the highly concentrated $NaClO_4$ electrolyte, sodium ions may react with dissolved O_2 and CO_2 gases at the potential near the Na intercalation of $NaTi_2(PO_4)_3$ (~2.1 V *vs.* Na/Na^+) via the following reaction sequence [39,60–63]:

$$Na^+ + O_2 + e^- \rightarrow NaO_2 \quad E^\circ = 2.27\,V\,(vs.\,Na/Na^+) \qquad (1)$$

$$2Na^+ + O_2 + 2e^- \rightarrow Na_2O_2 \quad E^\circ = 2.33\,V\,(vs.\,Na/Na^+) \tag{2}$$

$$4Na^+ + 3CO_2 + 4e^- \rightarrow 2Na_2CO_3 + C \quad E^\circ = 2.35\,V\,(vs.\,Na/Na^+) \tag{3}$$

While these reactions are expected to occur for both 1 m and 17 m electrolyte systems, thus initially forming a similar surface layer comprising of sodium carbonates and oxides, it is believed that the surface layer cannot be sustained in 1 m $NaClO_4$ electrolyte due to their general instability in water. It is widely known that they rapidly dissolve and hydrolyze in water via the following reactions [39,64,65]:

$$NaO_2 + 2H_2O \rightarrow Na^+(aq) + 4OH^-(aq) \tag{4}$$

$$Na_2O_2 + 2H_2O \rightarrow 2Na^+(aq) + 4OH^-(aq) \tag{5}$$

$$Na_2CO_3 + H_2O \rightarrow HCO_3^-(aq) + 2Na^+(aq) + OH^-(aq) \tag{6}$$

In fact, Na-O compounds in the surface layer readily hydrolyze and eventually form NaOH via the first two reactions [4] and [5], regardless of salt concentration in aqueous electrolyte, due to their instability in water. Unlike the case of high-concentration electrolytes, where the activity of the free water is significantly diminished, the dissolution reactions of NaOH and Na_2CO_3 are likely to occur rapidly in 1 m $NaClO_4$ electrolyte due to the substantial presence of free water. As a counter experiment to prove this, we investigated whether the surface layer composed of Na_2CO_3 and NaOH that formed after the cycling in the 17 m $NaClO_4$ electrolyte would be easily washed out in the fresh deionized (DI) water. In Fig. S8, it is shown that, after DI water washing, the amorphous layer on the surface of the electrode cycled in the electrolytes disappeared, with its thickness rapidly diminishing from ~3–4 nm to ~1 nm. It clearly supports the idea that the highly concentrated $NaClO_4$ electrolyte effectively preserves the surface layer composed of carbonates and hydroxides on the anode surface from the dissolution. A consequence of not having a surface protective layer on a fully sodiated $Na_{1+x}Ti_2(PO_4)_3$ ($x \leq 2$) electrode in dilute electrolyte is the chemical side reaction that results in hydrogen evolution and the loss of sodium, such as self-discharge, as in the following reaction [28]:

$$xH_2O(1) + Na_{1+x}Ti_2(PO_4)_3 \rightarrow xNaOH(s) + NaTi_2(PO_4)_3(s) + 0.5xH_2(g) \tag{7}$$

To further confirm the stability of the surface layer, we examined the changes in the open-circuit voltages (OCVs) of the charged full-cell after 20 cycles at 1C in 1 m and 17 m $NaClO_4$ electrolytes, as shown in Fig. 4f. The cell cycled in the 17 m $NaClO_4$ electrolyte was stable for far longer than the cell cycled in 1 m $NaClO_4$ electrolyte. The OCV of the cell cycled in 17 m $NaClO_4$ electrolyte was stably sustained at a constant voltage of 1.08 V for more than 37 days (~900 h). In contrast, the cell cycled in 1 m $NaClO_4$ electrolyte experienced a drastic voltage drop after only 50 h, indicating rapid sodium loss from the sodiated anode via self-discharge, leading to hydrogen evolution. This differing stability of the OCVs for the 1 m and 17 m electrolytes can be attributed to the availability of the stable protective layer generated on the anode surface. As a reference, the OCV plot of the cell cycled in 9.26 m $NaCF_3SO_3$ electrolyte in Fig. 4f also shows the stable constant voltage of 1.08 V for 546 h, indicating that the enhanced stability of the high-concentration $NaClO_4$ electrolyte systems is partly due to the stabilized surface of the anode, as was previously demonstrated for the high-concentration $NaCF_3SO_3$ electrolyte systems [28].

Conclusion

We demonstrated for the first time the feasibility of using high-concentration electrolyte based on low-cost inorganic solutes to construct a high-performance aqueous cell. From the rational screening of the potential solutes with respect to the solubility, cost, and solvation strength according to the Hofmeister series, 17 m of $NaClO_4$ was chosen and employed in the sodium aqueous rechargeable batteries. It was successfully demonstrated that a $Na_4Fe_3(PO_4)_2(P_2O_7)/NaTi_2(PO_4)_3$ full-cell could operate with a high energy density of 36 Wh kg^{-1} and coulombic efficiency up to 99% at 1C for over 200 cycles, outperforming the state-of-the-art super-concentrated systems based on $NaCF_3SO_3$. This significant outcome is attributed to two key aspects of highly concentrated inorganic electrolytes: (1) expansion of the electrochemical stability window to up to 2.7 V by suppressing water decomposition and (2) robust surface layer formation. In particular, the formation of the surface layer composed of Na_2CO_3 and NaOH led to remarkable stability of the full-cell with extraordinary storage stability for ~900 h. In addition, we proposed a new mechanism of the surface layer formation on the anode involving the oxygen reduction in contrast to the conventional model of the reduction of the salts. It was found that the relative stability of this surface layer in the high-concentration electrolyte aids the stability of the electrode in the cell. Our findings on the new inorganic solutes suitable for the high-concentration aqueous electrolytes broaden our understanding on this new class of electrolyte systems and provide important guidance for the realization of low-cost high-voltage aqueous batteries.

Acknowledgements

This work was supported by the National Research Foundation of Korea (NRF) grant funded by the Korea government (MSIP) (No. 2018R1A2A1A05079249). Also, this research was supported by Creative Materials Discovery Program through the National Research Foundation of Korea (NRF) funded by the Ministry of Science, ICT and Future Planning (NRF-2017M3D1A1039553) this work was supported by Project Code. (IBS-R006-A2) Also, This work was supported by the World Premier Materials grant funded by the Korea government Ministry of Trade, Industry and Energy.

Data availability

The raw/processed data required to reproduce these findings cannot be shared at this time as the data also forms part of an ongoing study.

Appendix A. Supplementary data

Supplementary data to this article can be found online at https://doi.org/10.1016/j.mattod.2019.02.004.

References

[1] C. Liu et al., Advanced materials for energy storage, Adv. Mater. 22 (2010) E28–E62. https://onlinelibrary.wiley.com/doi/abs/10.1002/adma.200903328.

[2] B. Dunn et al., Electrical energy storage for the grid: a battery of choices, Science 334 (2011) 928. http://science.sciencemag.org/content/334/6058/928.abstract.

[3] D. Larcher, J.M. Tarascon, Towards greener and more sustainable batteries for electrical energy storage, Nat. Chem. 7 (2014) 19, https://doi.org/10.1038/nchem.2085.

[4] Y. Huang et al., Electrode materials of sodium-ion batteries toward practical application, ACS Energy Lett. 3 (2018) 1604–1612, https://doi.org/10.1021/acsenergylett.8b00609.

[5] N.-S. Choi et al., Challenges facing lithium batteries and electrical double-layer capacitors, Angew. Chem. Int. Ed. 51 (2012) 9994–10024. https://onlinelibrary.wiley.com/doi/abs/10.1002/anie.201201429.

[6] J. Kalhoff et al., Safer electrolytes for lithium-ion batteries: state of the art and perspectives, ChemSusChem 8 (2015) 2154–2175. https://onlinelibrary.wiley.com/doi/abs/10.1002/cssc.201500284.

[7] H. Kim et al., Recent progress in electrode materials for sodium-ion batteries, Adv. Energy Mater. 6 (2016) 1600943. https://onlinelibrary.wiley.com/doi/abs/10.1002/aenm.201600943.

[8] E.P. Roth, C.J. Orendorff, How electrolytes influence battery safety, Electrochem. Soc. Interface 21 (2012) 45–49. http://interface.ecsdl.org/content/21/2/45.abstract.

[9] H. Vikström et al., Lithium availability and future production outlooks, Appl. Energy 110 (2013) 252–266. http://www.sciencedirect.com/science/article/pii/S0306261913002997.

[10] K. Xu, Nonaqueous liquid electrolytes for lithium-based rechargeable batteries, Chem. Rev. 104 (2004) 4303–4418, https://doi.org/10.1021/cr030203g.

[11] D. Bin et al., Progress in aqueous rechargeable sodium-ion batteries, Adv. Energy Mater. 8 (2018) 1703008. https://onlinelibrary.wiley.com/doi/abs/10.1002/aenm.201703008.

[12] H. Kim et al., Aqueous rechargeable Li and Na ion batteries, Chem. Rev. 114 (2014) 11788–11827, https://doi.org/10.1021/cr500232y.

[13] W. Tang et al., Aqueous rechargeable lithium batteries as an energy storage system of superfast charging, Energy Environ. Sci. 6 (2013) 2093–2104, https://doi.org/10.1039/C3EE24249H.

[14] S. Chen et al., High-voltage lithium-metal batteries enabled by localized high-concentration electrolytes, Adv. Mater. 30 (2018) 1706102. https://onlinelibrary.wiley.com/doi/abs/10.1002/adma.201706102.

[15] S. Jiao et al., Stable cycling of high-voltage lithium metal batteries in ether electrolytes, Nat. Energy 3 (2018) 739–746, https://doi.org/10.1038/s41560-018-0199-8.

[16] J. Qian et al., High rate and stable cycling of lithium metal anode, Nat. Commun. 6 (2015) 6362, https://doi.org/10.1038/ncomms7362.

[17] L. Suo et al., A new class of Solvent-in-Salt electrolyte for high-energy rechargeable metallic lithium batteries, Nat. Commun. 4 (2013) 1481, https://doi.org/10.1038/ncomms2513.

[18] J. Wang et al., Superconcentrated electrolytes for a high-voltage lithium-ion battery, Nat. Commun. 7 (2016) 12032, https://doi.org/10.1038/ncomms12032.

[19] J. Wang et al., Fire-extinguishing organic electrolytes for safe batteries, Nat. Energy 3 (2018) 22–29, https://doi.org/10.1038/s41560-017-0033-8.

[20] K. Yoshida et al., Oxidative-stability enhancement and charge transport mechanism in glyme-lithium salt equimolar complexes, J. Am. Chem. Soc. 133 (2011) 13121–13129, https://doi.org/10.1021/ja203983r.

[21] R.S. Kühnel et al., "Water-in-salt" electrolytes enable the use of cost-effective aluminum current collectors for aqueous high-voltage batteries, Chem. Commun. 52 (2016) 10435–10438, https://doi.org/10.1039/C6CC03969C.

[22] R.-S. Kühnel et al., A high-voltage aqueous electrolyte for sodium-ion batteries, ACS Energy Lett. 2 (2017) 2005–2006, https://doi.org/10.1021/acsenergylett.7b00623.

[23] D.P. Leonard et al., Water-in-salt electrolyte for potassium-ion batteries, ACS Energy Lett. 3 (2018) 373–374, https://doi.org/10.1021/acsenergylett.8b00009.

[24] M.R. Lukatskaya et al., Concentrated mixed cation acetate "water-in-salt" solutions as green and low-cost high voltage electrolytes for aqueous batteries, Energy Environ. Sci. (2018), https://doi.org/10.1039/C8EE00833G.

[25] D. Reber et al., High-voltage aqueous supercapacitors based on NaTFSI, Sustain. Energy Fuels 1 (2017) 2155–2161, https://doi.org/10.1039/C7SE00423K.

[26] L. Suo et al., "Water-in-salt" electrolyte enables high-voltage aqueous lithium-ion chemistries, Science 350 (2015) 938. http://science.sciencemag.org/content/350/6263/938.abstract.

[27] L. Suo et al., Advanced high-voltage aqueous lithium-ion battery enabled by "Water-in-Bisalt" electrolyte, Angew. Chem. Int. Ed. 55 (2016) 7136–7141. https://onlinelibrary.wiley.com/doi/abs/10.1002/anie.201602397.

[28] L. Suo et al., "Water-in-Salt" electrolyte makes aqueous sodium-ion battery safe, green, and long-lasting, Adv. Energy Mater. 7 (2017) 1701189. https://onlinelibrary.wiley.com/doi/abs/10.1002/aenm.201701189.

[29] F. Wang et al., Hybrid aqueous/non-aqueous electrolyte for safe and high-energy Li-ion batteries, Joule 2 (2018) 927–937. http://www.sciencedirect.com/science/article/pii/S2542435118300576.

[30] F. Wang et al., Highly reversible zinc metal anode for aqueous batteries, Nat. Mater. 17 (2018) 543–549, https://doi.org/10.1038/s41563-018-0063-z.

[31] Y. Yamada et al., Hydrate-melt electrolytes for high-energy-density aqueous batteries, Nat. Energy 1 (2016) 16129, https://doi.org/10.1038/nenergy.2016.129.

[32] C. Yang et al., 4.0 V aqueous Li-ion batteries, Joule 1 (2017) 122–132. http://www.sciencedirect.com/science/article/pii/S254243511730034X.

[33] C. Yang et al., Unique aqueous Li-ion/sulfur chemistry with high energy density and reversibility, Proc. Natl. Acad. Sci. 114 (2017) 6197. http://www.pnas.org/content/114/24/6197.abstract.

[34] Y. Marcus, Thermodynamics of solvation of ions. Part 5. —Gibbs free energy of hydration at 298.15 K, J. Chem. Soc. Faraday Trans. 87 (1991) 2995–2999, https://doi.org/10.1039/FT9918702995.

[35] B. Hribar et al., How ions affect the structure of water, J. Am. Chem. Soc. 124 (2002) 12302–12311, https://doi.org/10.1021/ja026014h.

[36] Y. Marcus, Effect of ions on the structure of water: structure making and breaking, Chem. Rev. 109 (2009) 1346–1370, https://doi.org/10.1021/cr8003828.

[37] E. Brini et al., How water's properties are encoded in its molecular structure and energies, Chem. Rev. 117 (2017) 12385–12414, https://doi.org/10.1021/acs.chemrev.7b00259.

[38] O. Borodin et al., Liquid structure with nano-heterogeneity promotes cationic transport in concentrated electrolytes, ACS Nano 11 (2017) 10462–10471, https://doi.org/10.1021/acsnano.7b05664.

[39] L. Suo et al., How solid-electrolyte interphase forms in aqueous electrolytes, J. Am. Chem. Soc. 139 (2017) 18670–18680, https://doi.org/10.1021/jacs.7b10688.

[40] F. Hofmeister, Zur Lehre von der Wirkung der Salze, Archiv für experimentelle Pathologie und Pharmakologie 24 (1888) 247–260, https://doi.org/10.1007/BF01918191.

[41] Y. Zhang, P.S. Cremer, Interactions between macromolecules and ions: the Hofmeister series, Curr. Opin. Chem. Biol. 10 (2006) 658–663. http://www.sciencedirect.com/science/article/pii/S1367593106001517.

[42] J.-H. Choi, M. Cho, Ion aggregation in high salt solutions. II. Spectral graph analysis of water hydrogen-bonding network and ion aggregate structures, J. Chem. Phys. 141 (2014) 154502, https://doi.org/10.1063/1.4897638.

[43] S. Kim et al., Ion aggregation in high salt solutions: Ion network versus ion cluster, J. Chem. Phys. 141 (2014), https://doi.org/10.1063/1.4896227 124510.

[44] J.-H. Choi, M. Cho, Ion aggregation in high salt solutions. IV. Graph-theoretical analyses of ion aggregate structure and water hydrogen bonding network, J. Chem. Phys. 143 (2015). 104110. 10.1063/1.4930608.

[45] J.-H. Choi et al., Ion aggregation in high salt solutions. III. Computational vibrational spectroscopy of HDO in aqueous salt solutions, J. Chem. Phys. 142 (2015), https://doi.org/10.1063/1.4920972 204102.

[46] J.-H. Choi, M. Cho, Ion aggregation in high salt solutions. VI. Spectral graph analysis of chaotropic ion aggregates, J. Chem. Phys. 145 (2016) 174501, https://doi.org/10.1063/1.4966246.

[47] J.-H. Choi et al., Ion aggregation in high salt solutions. VII. The effect of cations on the structures of ion aggregates and water hydrogen-bonding network, J. Chem. Phys. 147 (2017) 154107, https://doi.org/10.1063/1.4993479.

[48] B. Auer et al., Hydrogen bonding and Raman, IR, and 2D-IR spectroscopy of dilute HOD in liquid D_2O, Proc. Natl. Acad. Sci. 104 (2007) 14215. http://www.pnas.org/content/104/36/14215.abstract.

[49] B.M. Auer, J.L. Skinner, IR and Raman spectra of liquid water: theory and interpretation, J. Chem. Phys. 128 (2008) 224511, https://doi.org/10.1063/1.2925258.

[50] Y. Chen et al., ATR-FTIR spectroscopic studies on aqueous $LiClO_4$, $NaClO_4$, and $Mg(ClO_4)_2$ solutions, Phys. Chem. Chem. Phys. 6 (2004) 537–542, https://doi.org/10.1039/B311768E.

[51] A.G. Miller, J.W. Macklin, Vibrational spectroscopic studies of sodium perchlorate contact ion pair formation in aqueous solution, J. Phys. Chem. 89 (1985) 1193–1201, https://doi.org/10.1021/j100253a028.

[52] J.D. Coates, L.A. Achenbach, The Microbiology of Perchlorate Reduction and its Bioremediative Application

[53] H. Kim et al., New iron-based mixed-polyanion cathodes for lithium and sodium rechargeable batteries: combined first principles calculations and experimental study, J. Am. Chem. Soc. 134 (2012) 10369–10372, https://doi.org/10.1021/ja3038646.

[54] H. Kim et al., Understanding the electrochemical mechanism of the new iron-based mixed-phosphate $Na_4Fe_3(PO_4)_2(P_2O_7)$ in a Na rechargeable battery, Chem. Mater. 25 (2013) 3614–3622, https://doi.org/10.1021/cm4013816.

[55] A.J. Fernández-Ropero et al., Toward safe and sustainable batteries: $Na_4Fe_3(PO_4)_2P_2O_7$ as a low-cost cathode for rechargeable aqueous Na-ion batteries, J. Phys. Chem. C 122 (2018) 133–142, https://doi.org/10.1021/acs.jpcc.7b09803.

[56] S.I. Park et al., Electrochemical properties of $NaTi_2(PO_4)_3$ anode for rechargeable aqueous sodium-ion batteries, J. Electrochem. Soc. 158 (2011) A1067–A1070. http://jes.ecsdl.org/content/158/10/A1067.abstract.

[57] Z. Li et al., Towards high power high energy aqueous sodium-ion batteries: the $NaTi_2(PO_4)_3/Na_{0.44}MnO_2$ system, Adv. Energy Mater. 3 (2012) 290–294, https://doi.org/10.1002/aenm.201200598.

[58] X.-Y. Wu et al., Energetic aqueous rechargeable sodium-ion battery based on $Na_2CuFe(CN)_6$–$NaTi_2(PO_4)_3$ intercalation chemistry, ChemSusChem 7 (2014) 407–411, https://doi.org/10.1002/cssc.201301036.

[59] Y. Wang et al., A novel high capacity positive electrode material with tunnel-type structure for aqueous sodium-ion batteries, Adv. Energy Mater. 5 (2015) 1501005, https://doi.org/10.1002/aenm.201501005.

[60] P. Adelhelm et al., From lithium to sodium: cell chemistry of room temperature sodium–air and sodium–sulfur batteries, Beilstein J. Nanotechnol. 6 (2015) 1016–1055. http://www.ncbi.nlm.nih.gov/pmc/articles/PMC4419580/.

[61] X. Hu et al., Rechargeable room-temperature Na–CO_2 batteries, Angew. Chem. 128 (2016) 6592–6596, https://doi.org/10.1002/ange.201602504.

[62] J. Kim et al., Dissolution and ionization of sodium superoxide in sodium–oxygen batteries, Nat. Commun. 7 (2016) 10670, https://doi.org/10.1038/ncomms10670.

[63] X. Hu et al., Quasi–solid state rechargeable Na-CO_2 batteries with reduced graphene oxide Na anodes, Sci. Adv. 3 (2017). http://advances.sciencemag.org/content/3/2/e1602396.abstract.

[64] H. Yadegari et al., On rechargeability and reaction kinetics of sodium–air batteries, Energy Environ. Sci. 7 (2014) 3747–3757, https://doi.org/10.1039/C4EE01654H.

[65] C. Liu et al., On the stability of NaO_2 in Na–O_2 batteries, ACS Appl. Mater. Interfaces 10 (2018) 13534–13541, https://doi.org/10.1021/acsami.8b01516.